Bottomonium spectrum from lattice QCD with 2 + 1 flavors of domain wall fermions

Stefan Meinel*

*Department of Applied Mathematics and Theoretical Physics, University of Cambridge,
Centre for Mathematical Sciences, Cambridge CB3 0WA, United Kingdom*

Recently, realistic lattice QCD calculations with 2 + 1 flavors of domain wall fermions and the Iwasaki gauge action have been performed by the RBC and UKQCD Collaborations. Here, results for the bottomonium spectrum computed on their gauge configurations of size $24^3 \times 64$ with a lattice spacing of approximately 0.11 fm and four different values for the light quark mass are presented. Improved lattice nonrelativistic QCD is used to treat the b quarks inside the bottomonium. The results for the radial and orbital energy splittings are found to be in good agreement with experimental measurements, indicating that systematic errors are small. The calculation of the $\Upsilon(2S) - \Upsilon(1S)$ energy splitting provides an independent determination of the lattice spacing. For the most physical ensemble it is found to be $a^{-1} = 1.740(25)(19)$ GeV, where the first error is statistical/fitting and the second error is an estimate of the systematic errors due to the lattice nonrelativistic QCD action.

I. INTRODUCTION

Bottomonium mesons, the bound states of bottom quark-antiquark pairs, play an important role in the study of the strong interactions. The spectrum of bottomonium is known very well from experiment and there are many different approaches to calculating it theoretically. Lattice QCD provides a model-independent and accurate way of doing this.

One of the most important steps toward realistic lattice QCD calculations was the inclusion of dynamical light (u, d, and s) sea quarks. For many quantities of phenomenological interest, lattice QCD now allows reliable nonperturbative calculations that were previously impossible. In order to further control systematic errors and increase the confidence in lattice results, it is crucial to consider several different lattice actions and thereby test universality.

The RBC and UKQCD Collaborations have recently started large-scale lattice QCD calculations [1–6] with dynamical domain wall fermions and renormalization-group-improved gauge actions. The domain wall fermion action [7–9] has an approximate chiral symmetry that becomes exact, even at finite lattice spacing, when the extent L_s of the auxiliary fifth dimension is taken to infinity. This leads to better control over the renormalization of operators, a reduction of discretization errors, and more reliable chiral extrapolations.

The gauge configurations created by the RBC and UKQCD Collaborations have been made publicly available. In this work, the ensembles of size $24^3 \times 64$, $L_s = 16$ described in detail in [4] were used to compute the spectrum of bottomonium. Chiral symmetry is not as important for bottomonium as it is for light hadrons, but the calculations presented here nevertheless provide useful tests of the recent lattice calculations by the RBC and UKQCD

Collaborations. In particular, they provide an independent determination of the lattice spacing and a good way of tuning the b quark mass. The value of the bare b quark mass obtained here can also be used in lattice QCD calculations for heavy-light hadrons such as B mesons, which are of considerable importance for the phenomenology of weak decays and tests of the standard model.

The b quark has a mass larger than the inverse lattice spacing, so that the standard lattice actions as used for light quarks are not suitable to describe it. A preliminary calculation of the bottomonium spectrum on the RBC/UKQCD gauge configurations using a relativistic heavy-quark action was presented in [10]. Here, improved nonrelativistic QCD (NRQCD) [11–13] is employed instead, following closely the methods used in the calculation of the bottomonium spectrum on the MILC gauge configurations in [14] (these configurations use an improved staggered fermion action for the sea quarks and a one-loop Symanzik-improved gluon action).

The lattice calculation and analysis methods are described in detail in Sec. II. The results for the tuning of the b quark mass and tests of the dispersion relation are given in Secs. III A and III B, respectively. In Sec. III C, the results for the radial and orbital energy splittings as well as the lattice spacing are presented, followed by the fine and hyperfine structure in Sec. III D.

II. THE LATTICE CALCULATION

A. Lattice actions and parameters

The details of the domain wall fermion and Iwasaki gauge actions as used by the RBC and UKQCD Collaborations are given in [1]. Here, the gauge configurations of size $24^3 \times 64$ as described in [4] were used. These have $L_s = 16$, $\beta = 2.13$ and the strange quark mass is $am_s = 0.04$. There are ensembles with four different values for the degenerate light (up and down) quark

*S.Meinel@damtp.cam.ac.uk

TABLE I.   The ensembles of RBC/UKQCD gauge configura-
tions used here.

am_l	u_{0L}	MD range (step)	n_{conf}
0.005	0.8439	915–8665 (25)	311
0.01	0.8439	1475–8525 (25)	283
0.02	0.8433	1800–3600 (25)	73
0.03	0.8428	1275–3050 (25)	72

mass am_l, as shown in Table I. The "measurements" in
this work were started at the same molecular dynamics
(MD) time as in [4] to ensure complete thermalization.
Note however that the $am_l = 0.005$ and $am_l = 0.01$ en-
sembles have since been extended and the additional con-
figurations were included here. Measurements were
performed every 25 steps of MD time, as discussed further
in Sec. II C 4.

The lattice NRQCD action for the b quark is the same as
in the previous study of the bottomonium spectrum in [14],
with stability parameter $n = 2$. The full details of the
action can be found in e.g. [15]. After the initial tuning,
which will be described in Sec. III, the bare b quark mass
was set to $am_b = 2.536$.

All couplings in the NRQCD action are set to their tree-
level values, but the action is tadpole improved [16], which
accounts for a large amount of the renormalization. The
mean link in Landau gauge u_{0L} is used as the tadpole
improvement parameter; the values of u_{0L} for the different
ensembles are listed in Table I.

The NRQCD action in use includes relativistic correc-
tion terms up to order $\mathcal{O}(v^4)$ where v is the internal speed
of the b quarks inside the meson. For bottomonium, one
has $v^4 \approx 0.01$. The action is also tree-level Symanzik
improved. Systematic errors depend strongly on the ob-
servable under consideration and will be discussed indi-
vidually in Sec. III. However, finite-volume errors are
expected to be negligible in all cases due to the small
size of the bottomonium mesons.

B. Calculation of the meson two-point functions

As in [13], the heavy-heavy meson correlators with
momentum $\boldsymbol{p}$ were computed from

$$C(\Gamma_{sk}, \Gamma_{sc}, \boldsymbol{p}, t - t') = \sum_{\boldsymbol{x}_1, \boldsymbol{x}_2} \text{Tr}[G^\dagger(\boldsymbol{x}_1, t, \boldsymbol{x}_1', t')\Gamma_{sk}^\dagger(\boldsymbol{x}_1 - \boldsymbol{x}_2)$$
$$\times \tilde{G}_{sc}(\boldsymbol{x}_2, t, \boldsymbol{x}_1', t')]e^{-i\boldsymbol{p}[(\boldsymbol{x}_1 + \boldsymbol{x}_2)/2]}, \quad (1)$$

where $t > t'$ and

$$\tilde{G}_{sc}(\boldsymbol{x}_2, t, \boldsymbol{x}_1', t') = \sum_{\boldsymbol{x}_2'} G(\boldsymbol{x}_2, t, \boldsymbol{x}_2', t')\Gamma_{sc}(\boldsymbol{x}_1' - \boldsymbol{x}_2')$$
$$\times e^{i\boldsymbol{p}[(\boldsymbol{x}_1' + \boldsymbol{x}_2')/2]}. \quad (2)$$

In Eqs. (1) and (2), which are understood to be for a single
gauge configuration, G denotes the heavy-quark propaga-
tor which is 2×2 matrix valued in spinor space and 3×3
matrix valued in color space. The functions $\Gamma_{sc/sk}$ are the
"smearing functions" at source and sink, respectively,
which are also 2×2 matrix valued in spinor space. No
gauge links were included in $\Gamma_{sc/sk}$; instead the gauge
configurations were fixed to the Coulomb gauge.

In Table II the bottomonium states considered in this
work are listed, together with their continuum quantum
numbers, smearing functions $\Gamma(\boldsymbol{r})$ and representations of
the octahedral group [17]. As can be seen in the table, all
representations are chosen to be different, so that no mix-
ing is expected here. The radial functions $\phi_{nS}(\boldsymbol{r})$, $\phi_{nP}(\boldsymbol{r})$,
and $\phi_{nD}(\boldsymbol{r})$ for the nth radially excited S-wave ($L = 0$),
P-wave ($L = 1$), and D-wave ($L = 2$) states were taken
from the corresponding hydrogen atom wave functions and
are given in Table III. The same lattice representations
were used at source and sink but the radial smearing
functions were allowed to be different. The smearing pa-
rameters r_0 (in lattice units) were set to 1.0 ($1S$), 0.8 ($2S$),
0.6 ($3S$), 0.5 ($1P$), 0.4 ($2P$), and 0.5 ($1D$), respectively.

Note that $\tilde{G}$ in Eq. (2) can be computed efficiently by
using the function

$$\Gamma_{sc}(\boldsymbol{x}_1' - \boldsymbol{x}_2')e^{i\boldsymbol{p}[(\boldsymbol{x}_1' + \boldsymbol{x}_2')/2]} \quad (3)$$

as the initial condition in the heavy-quark evolution equa-
tion. For some states it is computationally more convenient
to remove the Pauli matrix in Γ_{sc} in the initial condition,
and instead include it explicitly in the trace in Eq. (1). In
this way, different spin directions can be obtained with a
single $\tilde{G}$.

TABLE II.   The smearing functions $\Gamma(\boldsymbol{r})$. See e.g. [17] for the irreducible representations of the octahedral group.

Name	L	S	J	P	C	Lattice rep. $\mathcal{R}^{PC}$	$\Gamma(\boldsymbol{r})$
$\eta_b(nS)$	0	0	0	−	+	A_1^{-+}	$\phi_{nS}(\boldsymbol{r})$
$\Upsilon(nS)$	0	1	1	−	−	T_1^{--}	$\phi_{nS}(\boldsymbol{r})\sigma^i$
$h_b(nP)$	1	0	1	+	−	T_1^{+-}	$\phi_{nP}(\boldsymbol{r})r^i/r_0$
$\chi_{b0}(nP)$	1	1	0	+	+	A_1^{++}	$\phi_{nP}(\boldsymbol{r})(\boldsymbol{r} \cdot \boldsymbol{\sigma})/r_0$
$\chi_{b1}(nP)$	1	1	1	+	+	T_1^{++}	$\phi_{nP}(\boldsymbol{r})(\boldsymbol{r} \times \boldsymbol{\sigma})^i/r_0$
$\chi_{b2}(nP)$	1	1	2	+	+	T_2^{++}	$\phi_{nP}(\boldsymbol{r})(r^i\sigma^j + r^j\sigma^i)/r_0$ $(i \neq j)$
$\eta_b(nD)$	2	0	2	−	+	T_2^{-+}	$\phi_{nD}(\boldsymbol{r})r^ir^j/r_0^2$ $(i \neq j)$
$\Upsilon_2(nD)$	2	1	2	−	−	E^{--}	$\phi_{nD}(\boldsymbol{r})(r^ir^j\sigma^k - r^jr^k\sigma^i)/r_0^2$ $(i \neq j, k \neq j)$

TABLE III. The radial functions $\phi(\mathbf{r})$.

State	$\phi(\mathbf{r})$
1S	$\exp[-|\mathbf{r}|/r_0]$
2S	$[1 - |\mathbf{r}|/(2r_0)]\exp[-|\mathbf{r}|/(2r_0)]$
3S	$[1 - 2|\mathbf{r}|/(3r_0) + 2|\mathbf{r}|^2/(27r_0^2)]\exp[-|\mathbf{r}|/(3r_0)]$
1P	$\exp[-|\mathbf{r}|/(2r_0)]$
2P	$[1 - |\mathbf{r}|/(6r_0)]\exp[-|\mathbf{r}|/(3r_0)]$
1D	$\exp[-|\mathbf{r}|/(3r_0)]$

Finally, note that on a finite lattice, the smearing functions must satisfy the periodic boundary conditions. This was ensured by setting the smearing functions to zero outside a ball with radius R smaller than half the spatial lattice dimension. In this way, the wrapping around the lattice boundaries does not cause any problems. Since the smearing functions decay exponentially with the separation between quark and antiquark, R can be chosen such that the important features remain. To ensure symmetry, the same cutoff radius must be taken at source and sink.

In order to increase statistics, the correlators (1) were averaged over eight different spatial origins $\mathbf{x}'_1$ located at the corners of a cube with side length $L/2 = 12$. In addition, four different source time slices t' with an equal spacing of 16 were used, thus leading to a total of 32 origins per configuration. Furthermore, the locations of the origins on the lattice were shifted randomly from configuration to configuration in order to decrease autocorrelations.

C. Fitting and analysis details

1. Bayesian multiexponential fitting

After choosing a set of smearing functions $\Gamma(\mathbf{r})$ with equal lattice representations but different radial functions (e.g. 1S, 2S, and 3S), the square matrix of correlators obtained by taking all combinations for source and sink was computed.

The matrix of correlators $\langle C(\Gamma_{\text{sk}}, \Gamma_{\text{sc}}, \mathbf{p}, t - t') \rangle$ was simultaneously fitted by a function of the form

$$\sum_{n=0}^{n_{\exp}-1} A_n(\Gamma_{\text{sc}})A_n^*(\Gamma_{\text{sk}})e^{-E_n(t-t')}, \tag{4}$$

where E_n is the energy of the nth state and $A_n(\Gamma)$ is the (real) amplitude for this state to be created by the operator with smearing function $\Gamma(\mathbf{r})$.

To ensure the correct ordering of the states in terms of their energy, the fit parameters were actually chosen to be the logarithms of the energy differences between neighboring states (in lattice units)

$$\ln(E_{n+1} - E_n) \tag{5}$$

and the logarithm of the ground state energy, $\ln(E_0)$. Furthermore, the amplitudes for the excited states were

written as

$$A_n(\Gamma) = A'_n(\Gamma)A_0(\Gamma), \tag{6}$$

taking the relative amplitudes $A'_n(\Gamma)$ (for $n \geq 1$) and the ground state amplitude $A_0(\Gamma)$ as the fit parameters.

The Bayesian fitting method described in [18] was used, where the χ^2 function is augmented by

$$\chi^2 \rightarrow \chi^2 + \chi^2_{\text{prior}} \tag{7}$$

with the Gaussian prior

$$\chi^2_{\text{prior}} = \sum_i \frac{(p_i - \tilde{p}_i)^2}{\sigma^2_{\tilde{p}_i}}. \tag{8}$$

Here, $\{p_i\} = \{A_0(\Gamma), A'_n(\Gamma), \ln(E_0), \ln(E_{n+1} - E_n)\}$ are the fitting parameters, and the prior for each parameter p_i is given by its central value $\tilde{p}_i$ and width $\sigma_{\tilde{p}_i}$.

The Bayesian method allows the inclusion of an arbitrary number of exponentials $n_{\exp}$ in (4) and hence the fitting in the full range of Euclidean time $t - t'$ between source and sink. Here, only the points with $t - t' = 0$ were excluded in the fits. The number of exponentials is increased until the fit results and error estimates become independent of $n_{\exp}$. This is demonstrated in Fig. 1.

In the following discussion of the prior choices $\{\tilde{p}_i, \sigma_{\tilde{p}_i}\}$ we will distinguish between parameters for *low-lying* and *high-lying* states. For example, in a 3×3 matrix fit containing sources optimized for the $\Upsilon(1S)$, $\Upsilon(2S)$, and $\Upsilon(3S)$ states, these three states will be referred to as low lying, as their energies and amplitudes will be well determined by the data, while higher excitations will be referred to as high lying.

The prior widths for the parameters of the low-lying states were chosen to be about 10 times larger than the
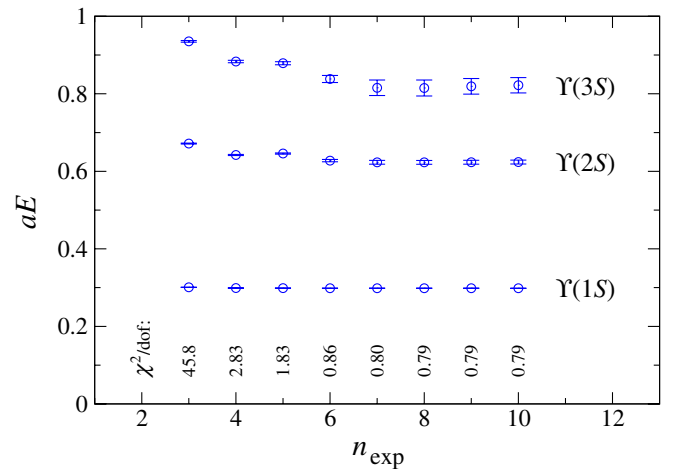

FIG. 1 (color online). Fit results for the 3×3 matrix correlator with the $\{\Upsilon(1S), \Upsilon(2S), \Upsilon(3S)\}$ smearings as a function of the number of exponentials. The values of χ^2 divided by the number of degrees of freedom are also shown. The results are for the ensemble with $am_l = 0.005$.

resulting error estimates from the fit. This ensures that the influence of the priors on these parameters is negligible. Initial guesses for the central values were obtained from unconstrained fits including only a small number of exponentials at large Euclidean time.

For the high-lying states, the priors for the logarithms of the energy splittings between successive states, $\ln(E_{n+1} - E_n)$, were set to -1.4 (corresponding to about 400 MeV) with a width of 1. The priors for the relative amplitudes $A'_n(\Gamma)$ of the high-lying states were set to zero with a width of 5.

2. NRQCD energy shift

Because of the use of lattice NRQCD, where the heavy-quark mass has been integrated out of the action, all energies obtained from the fits are shifted,

$$E = E_{\mathrm{phys}} - 2C \qquad (9)$$

where C is approximately equal to the heavy-quark mass. Since C is the same for all states, energy splittings are unaffected by this shift.

The physical mass of a meson (and hence C) can be calculated from the energy difference between its states with $\boldsymbol{p} = 0$ and $\boldsymbol{p} \neq 0$. Assuming the relativistic continuum dispersion relation

$$E(\boldsymbol{p}) = \sqrt{\boldsymbol{p}^2 + M^2} - 2C \qquad (10)$$

we obtain the *kinetic mass*

$$M = M_{\mathrm{kin}} \equiv \frac{\boldsymbol{p}^2 - [E(\boldsymbol{p}) - E(0)]^2}{2[E(\boldsymbol{p}) - E(0)]}. \qquad (11)$$

With the improved lattice actions used in this work, the continuum dispersion relation (10) was found to be an excellent approximation for bottomonium at small lattice momenta $\boldsymbol{p}$. This will be demonstrated in Sec. III B.

3. Bootstrap method

When computing quantities that depend on more than one fit result, such as the kinetic mass (11) or an energy splitting obtained from independent fits, correlations between the different fit results must be taken into account. In this work, the bootstrap method was employed to achieve this. Note however that it must be modified for Bayesian fitting [18] so that not only the data sets are resampled randomly but also the central values $\tilde{p}_i$ of the priors in (8) are drawn from Gaussian random distributions with widths $\sigma_{\tilde{p}_i}$ for every fit.

The final quantity of interest is then computed for the bootstrap ensemble of fit results, giving an approximate probability distribution. In the end, the mean value and the 68% width of this distribution are quoted.

The bootstrap method was in fact not only used for quantities depending on more than one fit parameter but

also to obtain the error estimates for individual fit parameters. The number of bootstrap samples was taken to be 500.

4. Autocorrelations

The integrated autocorrelation time τ_{int} for the 12th time slice of the pion correlator on the $am_l = 0.005$ ensemble was found to be 10 to 15 steps of MD time in [4]. Therefore only gauge configurations separated by 25 steps, which is approximately equal to $2\tau_{\mathrm{int}}$, were used here. However, the autocorrelation time depends on the observable. The measurements in this work were checked for residual autocorrelations using the binning method.

Recall from Sec. II B that on each gauge configuration meson correlators from 32 origins (8 origins on 4 source time slices each) were computed. The data were always averaged over the 8 origins on each source time slice, thus leaving 4 data samples per configuration.

To estimate the autocorrelations between the different gauge configurations, the data were also averaged over the 4 source time slices prior to the binning. Note that the measurements already had an initial separation of 25 steps in MD time, and hence the binning increases this to integer multiples of 25.

Of course the binning reduces the number of data samples available for the fit. To obtain a reliable estimate of the data covariance matrix (see e.g. [18]), the number of data samples should be much larger than the dimension of this matrix. Thus, in the analysis of autocorrelations, fits with only one smearing at source and sink and a small fitting range, corresponding to a small data covariance matrix, were considered.

No significant increases in the bootstrap errors were seen for any of the ensembles, indicating that the separation of 25 steps of MD time gives sufficiently independent measurements. Note that the origins of the meson correlators were shifted randomly between gauge configurations.

Next, tests for autocorrelations between the data samples from the four different source time slices were performed. To this end the data were averaged into bins of 2 or 4 time slices, without additional binning over gauge configurations. Here, in some cases a slight increase in the bootstrap errors was seen, at most 20%. Thus, for the measurements in the remainder of this work the following conventions were used: on the $am_l = 0.005$ and $am_l = 0.01$ ensembles all 4 source time slices were binned together, except for the 3×3 matrix correlator in the determination of the $\Upsilon(3S)$ energy. For the latter no binning over source time slices was done; instead the error estimates from the fits were corrected by 20% upward to be safe. For the $am_l = 0.02$ and $am_l = 0.03$ ensembles, which have about 4 times fewer configurations, the $\Upsilon(3S)$ state was not computed. There, for the 2×2 matrix correlators no binning over source time slices was performed, again increasing the error estimates by 20% upward instead. For the D-wave correlators, only the $1D$ smearing function was included in

the fits. Thus, the data covariance matrix was small and binning over all 4 source time slices was used.

III. RESULTS

A. Tuning the bare b quark mass

The bare b quark mass, which is a free parameter in the NRQCD action, was tuned nonperturbatively. It was adjusted such that the kinetic mass of the $\eta_b(1S)$ meson as calculated on the lattice matches the experimental value of 9.389(5) GeV [19]. The tuning was done on the most chiral ($am_l = 0.005$) ensemble of gauge configurations.

The kinetic mass was computed from (11), where the smallest possible lattice momentum $a|\boldsymbol{p}| = 1 \cdot 2\pi/L$ was used. As shown in the next section, the kinetic mass is very stable and shows no significant dependence on $\boldsymbol{p}$ even for much larger momenta. In order to increase statistics the results were averaged over the different possibilities for the direction of $\boldsymbol{p}$.

The comparison with experiment of course requires the knowledge of the lattice spacing, which was determined as the ratio of the experimentally measured $\Upsilon(2S) - \Upsilon(1S)$ mass splitting, 0.56296(40) GeV [20], to the dimensionless lattice result. This will be discussed in more detail in Sec. III C.

The lattice results for aM_{kin} and the $\Upsilon(2S) - \Upsilon(1S)$ splitting at the three different bare quark masses $am_b = 2.30, 2.45,$ and 2.60 are shown in Table IV. As can be seen, the $\Upsilon(2S) - \Upsilon(1S)$ splitting is very insensitive to the value of the b quark mass. It is also expected to have much smaller lattice discretization errors than the $1P - 1S$ splitting as discussed in the next section.

It was found that in the range considered here, the dependence of the kinetic mass on the bare heavy-quark mass is described very well by the linear relation

$$aM_{\text{kin}} = A + B \cdot am_b. \tag{12}$$

A plot of aM_{kin} as a function of am_b is shown in Fig. 2. Fits of Eq. (12) with the parameters A and B were performed on 500 bootstrap samples for the kinetic masses at $am_b = 2.30, 2.45,$ and 2.60. The resulting average fit parameters were

$$A = 0.489(25), \qquad B = 1.956(11). \tag{13}$$

To obtain a first result for the lattice spacing of the $am_l = 0.005$ ensemble, the $\Upsilon(2S) - \Upsilon(1S)$ mass splitting at

TABLE IV. Results for tuning of the bare b quark mass in lattice units. Errors are statistical/fitting only.

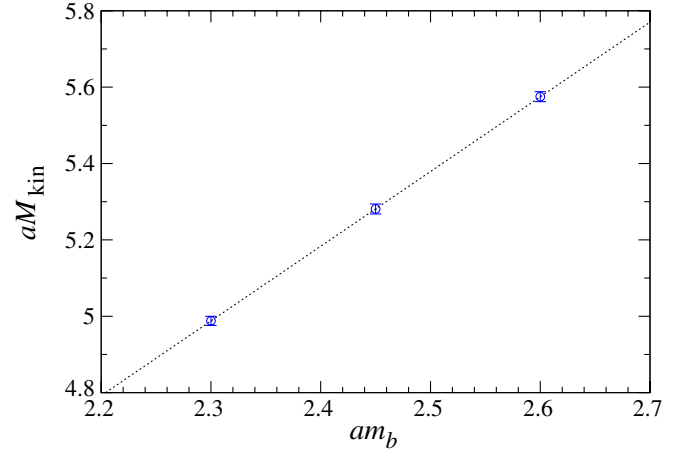| am_b	$aM_{\text{kin}}(\eta_b)$	$\Upsilon(2S) - \Upsilon(1S)$ splitting
2.30	4.988(12)	0.3258(47)
2.45	5.281(13)	0.3242(46)
2.60	5.575(13)	0.3231(54)

FIG. 2 (color online). The kinetic mass of the $\eta_b(1S)$ meson plotted against the bare heavy-quark mass. Errors are statistical/fitting only. The line shows the average over the bootstrap ensemble of linear fit results.

$am_b = 2.45$ was used, giving $a^{-1} = 1.736(25)$ GeV (the error is statistical/fitting only). Of course the b quark mass was not yet tuned, but given the relative independence of the $\Upsilon(2S) - \Upsilon(1S)$ splitting on m_b, the value of $am_b = 2.45$ was sufficiently close to the physical value. The final results for the lattice spacing obtained with the correct b quark mass will be presented in Sec. III C.

Using the preliminary result for a^{-1}, it follows that the $\eta_b(1S)$ mass in lattice units must be tuned to be $aM_{\text{kin}} = 5.407(77)$. Inserting this into (12) and solving for am_b gives

$$am_b = 2.514(36). \tag{14}$$

The error quoted here is statistical/fitting only and is dominated by the uncertainty in the lattice result for the $\Upsilon(2S) - \Upsilon(1S)$ splitting.

All remaining calculations were actually performed with $am_b = 2.536$. This was an earlier result and the fits have been improved slightly since then. However it is still inside the range of the new value (14).

For $am_b = 2.536$ the results were $aM_{\text{kin}} = 5.449(13)$ and $a^{-1} = 1.740(25)$ GeV. This gives $M_{\text{kin}} = 9.48(14)$ GeV which is compatible with the experimental result of 9.389(5) GeV, confirming the successful tuning of the heavy-quark mass.

Note that the lattice NRQCD action can be used for both heavy-heavy mesons and heavy-light hadrons. Thus, the result for the bare b quark mass obtained here will be useful also in future calculations for heavy-light hadrons.

B. Speed of light

In order to examine how well the lattice data approximate the relativistic continuum dispersion relation (10), the kinetic mass of the $\eta_b(1S)$ meson, defined by (11), was also computed for larger lattice momenta $a\boldsymbol{p} = \boldsymbol{n} \cdot 2\pi/L$

TABLE V. Kinetic mass, NRQCD energy shift, and the square of the "speed of light" for various lattice momenta $a\mathbf{p} = \mathbf{n} \cdot 2\pi/L$, calculated on the $am_l = 0.005$ ensemble with $am_b = 2.536$.

$\mathbf{n}^2$	$aM_{\text{kin}}(\eta_b)$	aC	c^2
1	5.450(17)	2.5913(84)	...
2	5.450(17)	2.5912(85)	1.000 03(85)
3	5.450(18)	2.5911(92)	1.000 1(16)
4	5.461(22)	2.597(11)	0.998 1(21)
5	5.457(20)	2.595(10)	0.998 7(24)
6	5.452(20)	2.592(10)	0.999 7(27)
8	5.454(22)	2.593(11)	0.999 3(35)
9	5.447(20)	2.590(10)	1.000 5(35)
12	5.445(21)	2.589(11)	1.000 9(42)

up to $\mathbf{n}^2 = 12$. For these calculations, the local smearing function $\Gamma(\mathbf{r}) = \delta_{\mathbf{r},0}$ was used at source and sink so that multiple lattice momenta can be obtained with little computational cost. For each value of $\mathbf{n}^2$, the results were averaged over the possible directions of the vector $\mathbf{n}$, and all components of $\mathbf{n}$ were chosen to be less than or equal to 2.

The results are given in Table V, where also the NRQCD energy shift, calculated as

$$C = \frac{M_{\text{kin}}(\mathbf{p}) - E(0)}{2}, \qquad (15)$$

and for $\mathbf{n}^2 > 1$ the square of the "speed of light"

$$c^2 \equiv \frac{[E(\mathbf{p}) - E(0) + M_{\text{kin},1}]^2 - M_{\text{kin},1}^2}{\mathbf{p}^2} \qquad (16)$$

are shown. In Eq. (16), $M_{\text{kin},1}$ denotes the kinetic mass calculated with $\mathbf{n}^2 = 1$. In the units used here, one should have $c^2 = 1$. Deviations of c^2 from 1 can be caused by discretization errors in the NRQCD, gluon, and sea quark actions and also by missing higher order relativistic corrections in the NRQCD action. The NRQCD action is highly improved at tree level, and so the most significant errors one expects here are those caused by missing radiative corrections.

As can be seen in the table, in the momentum range considered here the kinetic mass shows no significant

dependence on $\mathbf{p}$ within the small statistical/fitting errors. Correspondingly, c^2 remains compatible with 1, with statistical/fitting errors less than 0.5%, indicating that the effect of the errors mentioned above is small.

Analogous calculations for the $\Upsilon(1S)$ meson have been performed in [14] with the same NRQCD action but with the Lüscher-Weisz gluon and the AsqTad sea quark action. There, the deviation of c^2 from 1 in the same momentum range was also found to be compatible with 1 within statistical errors of less than 1%.

C. Radial/orbital splittings and the lattice spacing

The lattice results for the various radial and orbital energy splittings are listed in Table VI.

Systematic errors are known to be smallest for the spin-averaged masses, defined as

$$\langle M \rangle = \frac{\sum_J (2J + 1)M_J}{\sum_J (2J + 1)}. \qquad (17)$$

However, in most cases not all of the states entering Eq. (17) are known from experiment. For the $1S$, $2S$, and $3S$ masses in this section the $J = 1$ states (Υ) are considered instead of the spin averages. Note that the $J = 0$ S-wave states (η_b) enter the spin-averaged masses only with a weight of $1/4$, and so the influence of systematic errors in the hyperfine splittings is negligible here. For the $1P$ and $2P$ masses, the spin averages over the χ_b triplet ($J = 0, 1, 2$) states are used. The only experimentally known D-wave state [21] is $\Upsilon_2(1D)$ with $J = 2$, and this state is therefore considered here.

In terms of the NRQCD power counting [12], radial and orbital energy splittings are of order $\mathcal{O}(v^2)$, where v is the internal speed of the b quarks inside the heavy-heavy meson. For bottomonium one has $v^2 \approx 0.1$. The NRQCD action in use includes all relativistic corrections of order $\mathcal{O}(v^4)$ (at tree level), and hence the missing relativistic corrections are of order $\mathcal{O}(v^6)$. Naively this leads to relativistic errors for the radial and orbital splittings of $\mathcal{O}(v^4) = 1\%$. However, as discussed in [14], for energy splittings one has to consider the *difference* between the expectation values of the missing operators for the two

TABLE VI. Results for the radial and orbital energy splittings in lattice units. Errors are statistical/fitting only.

	$am_l = 0.005$	$am_l = 0.01$	$am_l = 0.02$	$am_l = 0.03$
$\Upsilon(2S) - \Upsilon(1S)$	0.3236(46)	0.3270(73)	0.330(18)	0.327(23)
$\Upsilon(3S) - \Upsilon(1S)$	0.517(21)	0.537(23)	...	...
$\langle \chi_b(1P) \rangle - \Upsilon(1S)$	0.2589(30)	0.2572(22)	0.2628(57)	0.2613(61)
$\langle \chi_b(2P) \rangle - \Upsilon(1S)$	0.478(30)	0.502(26)	0.511(39)	0.516(37)
$\langle \chi_b(2P) \rangle - \langle \chi_b(1P) \rangle$	0.219(29)	0.245(24)	0.248(35)	0.255(33)
$\Upsilon_2(1D) - \Upsilon(1S)$	0.4080(46)	0.4194(42)	0.417(12)	0.426(12)

TABLE VII. Estimates of the systematic errors due to the lattice NRQCD action for the $2S - 1S$ radial and $1P - 1S$ orbital splittings [14].

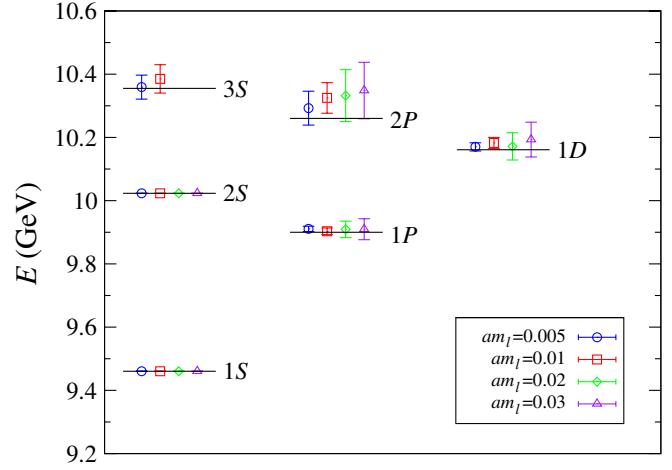|	$2S - 1S$	$1P - 1S$
Relativistic	0.5%	1.0%
Radiative	0.5%	1.7%
Discretization	0.8%	3.2%
Total	1.1%	3.8%

FIG. 3 (color online). Radial and orbital energy splittings compared to the experimental results (indicated by lines). Errors are statistical/fitting only and include the uncertainty in the determination of the lattice spacing. The $1S$ and $2S$ masses, for which no error bars are shown, are not predictions of the lattice calculation as these states are used to determine the lattice scale and the overall energy shift.

states. This leads to a reduction of the relativistic errors for the $2S - 1S$ splitting to about 0.5%.

Additional systematic errors for the NRQCD action are due to discretization errors and missing radiative corrections (beyond tadpole improvement). Estimates of these errors for the $2S - 1S$ and $1P - 1S$ splittings are given in Table VII. They are taken to be equal to the estimates obtained in [14] for exactly the same lattice NRQCD action on the "coarse" MILC gauge configurations, which have a lattice spacing ($a^{-1} \approx 1.6$ GeV) very similar to the ensembles considered here. The reader is referred to [14,22] for the details. As can be seen in the table, systematic errors are much smaller for the $2S - 1S$ splitting compared to the $1P - 1S$ splitting. This is due to the smaller difference in the wave functions for the $2S$ and $1S$ states. The $2S - 1S$ splitting thus allows a more reliable determination of the lattice spacing.

Note that there are also discretization errors due to the gluon and sea quark actions. These are difficult to quantify at this stage as only data from one lattice spacing are available. Gauge configurations with a smaller lattice spacing are currently being generated by the RBC and UKQCD Collaborations so that a more systematic analysis will become possible in the future. In [4], a preliminary error estimate of $(a\Lambda_{\mathrm{QCD}})^2 \approx 4\%$ for the calculations of light hadron properties on the current ensembles was given. The calculations performed here are different in that the domain wall action only enters via the sea quarks. The Iwasaki gluon action [23,24] is renormalization group improved and is therefore expected to have a better scaling behavior than the unimproved Wilson action. However, this depends on the observable considered; see e.g. [25] for a scaling study of the critical temperature and glueball masses. The stability of the speed of light demonstrated in Sec. III B provides some evidence for the smallness of the effect of gluon discretization errors for bottomonium.

For reference, the discretization errors in the $2S - 1S$ and $1P - 1S$ splittings on the coarse MILC lattices due to the Lüscher-Weisz gluon action were estimated in [14] to be 0.5% and 1.7%, respectively. These errors are proportional to the difference in the square of the wave function at the origin, which is smaller between the $2S$ and $1S$ states.

The results for the inverse lattice spacings of the four ensembles from both the $\Upsilon(2S) - \Upsilon(1S)$ and the $\langle \chi_b(1P) \rangle - \Upsilon(1S)$ splittings are listed in Table VIII. For the most chiral ensemble the $2S - 1S$ splitting gives $a^{-1} = 1.740(25)_{\mathrm{stat}}(19)_{\mathrm{syst}}$ GeV. No significant dependence on the sea quark mass can be seen within the statistical errors, and therefore no extrapolation was attempted. For comparison, the RBC and UKQCD Collaborations have obtained $a^{-1} = 1.729(28)_{\mathrm{stat}}$ in the chiral limit, using the Ω^- baryon mass [4]. This is consistent with the results obtained here.

Next, the lattice spacing determinations from the $2S - 1S$ splitting were used to convert the other radial and orbital splittings from Table VI to physical units. The results are plotted in Fig. 3. Note that the individual results for the lattice spacings of the different ensembles were used.

TABLE VIII. Results for the inverse lattice spacing obtained from the $\Upsilon(2S) - \Upsilon(1S)$ and $\langle \chi_b(1P) \rangle - \Upsilon(1S)$ splittings. The first error given is statistical/fitting and the second is an estimate of the systematic errors (relativistic, radiative, and discretization) due to the NRQCD action. Systematic errors due to the gluon and sea quark actions are not included.

	$am_l = 0.005$	$am_l = 0.01$	$am_l = 0.02$	$am_l = 0.03$
a^{-1}_{2S-1S} (GeV)	1.740(25)(19)	1.722(38)(19)	1.708(92)(19)	1.72(12)(2)
a^{-1}_{1P-1S} (GeV)	1.698(19)(65)	1.709(15)(65)	1.673(36)(64)	1.682(40)(64)

Overall, good agreement with experiment is seen. The dependence on the light sea quark mass is found to be weak. This is expected since the typical gluon momenta inside the bottomonium are much larger than all the values for the light quark masses used here. However, note that large deviations between lattice results and experiment were previously seen in quenched simulations ($n_f = 0$), so the inclusion of $2 + 1$ flavors of dynamical light quarks is in fact very important. A comparison between quenched and unquenched results can be found in [26].

D. Spin-dependent energy splittings

The spin-dependent energy splittings in bottomonium, i.e. the fine and hyperfine structure, are of order $\mathcal{O}(v^4)$ and hence any subleading corrections are missing in the NRQCD action used here. Therefore, the relativistic errors in these splittings are expected to be of order $\mathcal{O}(v^2) \approx 10\%$. The spin-dependent energy splittings also receive radiative corrections of order $\mathcal{O}(\alpha_s)$, the strong coupling constant at the scale set by the lattice spacing. This leads to further systematic errors of the order of 20%, although tadpole improvement reduces the problem. Finally, discretization errors are also expected to be larger than for the radial and orbital splittings, especially for the S-wave hyperfine splitting as discussed later.

The results for the spin-dependent energy splittings in lattice units are summarized in Table IX, where the errors given are statistical/fitting only.

1. S-wave hyperfine structure

Figure 4 shows a plot of the $\Upsilon(1S) - \eta_b(1S)$ and $\Upsilon(2S) - \eta_b(2S)$ energy splittings, where the previous lattice spacing determinations from the $2S - 1S$ splittings were used to convert to physical units.

The errors shown are statistical/fitting only but include the uncertainty in the determination of the lattice spacing. The latter in fact enters with a factor of 2 here, as discussed in [22], due to the resulting uncertainty in the physical heavy-quark mass (the hyperfine splitting is approximately
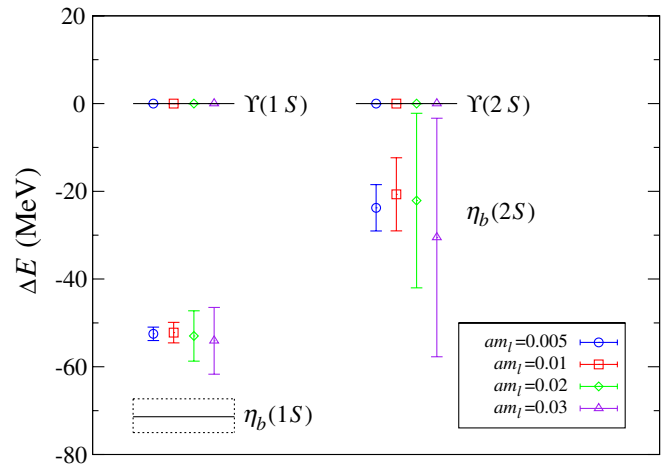

FIG. 4 (color online). S-wave hyperfine splittings [energies relative to the $\Upsilon(1S)$ and $\Upsilon(2S)$ states, respectively] compared to experiment. Errors are statistical/fitting only and include the uncertainty in the determination of the lattice spacing, which enters with a factor of 2. Large systematic errors are expected as discussed in the text.

proportional to the inverse of that mass). The statistical error in the $1S$ hyperfine splitting is then dominated by far by this uncertainty, while the $2S$ hyperfine splitting has an intrinsically higher statistical error as the state is radially excited.

The $\Upsilon(1S) - \eta_b(1S)$ splitting has recently been measured by the *BABAR* Collaboration [19], who found $71.4^{+2.3}_{-3.1}(\text{stat}) \pm 2.7(\text{syst})$ MeV. This value is indicated in Fig. 4. The lattice result in physical units for the $am_l = 0.005$ ensemble is $52.5 \pm 1.5(\text{stat})$ MeV, which is too small by about 25%, in line with the large systematic errors expected. Similarly to the radial and orbital splittings, little dependence on the light sea quark mass is seen, which is expected for the same reason as discussed there.

Note that in [14,22] a significant dependence on the lattice spacing was found, with the result increasing toward finer lattices, indicating that a substantial part of the deviation is due to discretization errors. The hyperfine split-

TABLE IX. Spin-dependent energy splittings in lattice units. Errors are statistical/fitting only. Large systematic errors are expected as discussed in the text.

	$am_l = 0.005$	$am_l = 0.01$	$am_l = 0.02$	$am_l = 0.03$
$\Upsilon(1S) - \eta_b(1S)$	0.03017(14)	0.03033(16)	0.03102(36)	0.03145(38)
$\Upsilon(2S) - \eta_b(2S)$	0.0137(30)	0.0120(48)	0.013(12)	0.018(16)
$\chi_{b0}(1P) - \langle\chi_b(1P)\rangle$	$-0.0207(20)$	$-0.0206(18)$	$-0.0231(36)$	$-0.0175(70)$
$\chi_{b1}(1P) - \langle\chi_b(1P)\rangle$	$-0.0049(14)$	$-0.0027(19)$	$-0.0059(22)$	$-0.0049(41)$
$\chi_{b2}(1P) - \langle\chi_b(1P)\rangle$	0.0071(11)	0.0058(12)	0.0082(17)	0.0064(29)
$h_b(1P) - \langle\chi_b(1P)\rangle$	$-0.0026(18)$	$-0.0002(21)$	$-0.0014(27)$	$-0.0058(42)$
$\chi_{b1}(1P) - \chi_{b0}(1P)$	0.0158(18)	0.0176(25)	0.0173(40)	0.0126(77)
$\chi_{b2}(1P) - \chi_{b1}(1P)$	0.0120(23)	0.0088(31)	0.0137(38)	0.0113(68)
$h_b(1P) - \chi_{b1}(1P)$	0.0023(16)	0.0027(16)	0.0044(35)	$-0.0009(61)$
$\Upsilon_2(1D) - \eta_b(1D)$	0.0011(21)	$-0.0012(18)$	$-0.0086(70)$	$-0.0050(61)$

ting is indeed expected to be sensitive to very short distances, as the spin-spin interaction potentials in simple models contain a delta function at the origin (see e.g. [27]).

Finally, note that in [10], where a relativistic heavy-quark action was used, the $\Upsilon(1S) - \eta_b(1S)$ splitting on the same RBC/UKQCD gauge configurations was found to be only $23.7 \pm 3.7(\text{stat})$ MeV, a much larger deviation to experiment than found here.

2. P-wave spin-dependent splittings

A plot of the $1P$ spin-dependent splittings, converted to physical units using the previous $2S - 1S$ lattice spacing results, is given in Fig. 5.

It shows the energy differences of the $\chi_{b0}(1P)$, $\chi_{b1}(1P)$, $\chi_{b2}(1P)$, and $h_b(1P)$ states to the spin average of the triplet $\langle\chi_b(1P)\rangle$. The experimental results [20] for the triplet states are also indicated in the plot; the h_b states have not yet been observed.

The lattice results are found to be in relatively good agreement with experiment, even within the purely statistical/fitting errors shown in the plot (those include the uncertainty in the lattice spacing). This indicates that discretization errors may be smaller than for the S-wave hyperfine splittings. Note that in simple potential models the wave function at the origin is zero (cf. the smearing functions in Table II) and hence the P-wave spin splittings are expected to be not as sensitive to very short distances as the S-wave hyperfine splittings.

The result for the experimentally unknown $h_b(1P) - \langle\chi_b(1P)\rangle$ splitting on the $am_l = 0.005$ ensemble is -4.5 ± 3.1 MeV, where the error quoted is statistical/fitting only and includes the uncertainty from the determination of the lattice spacing.
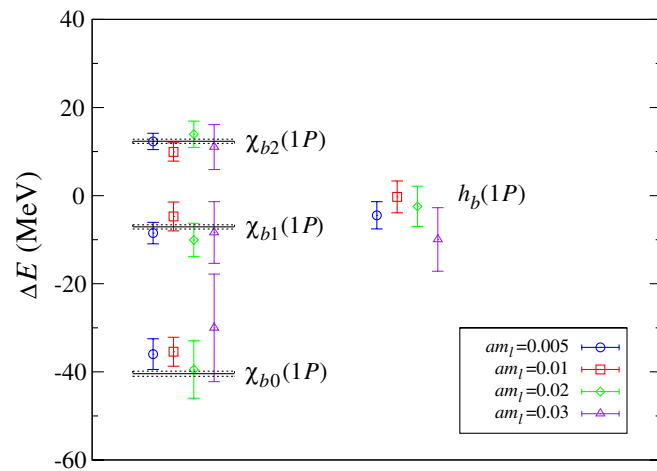

FIG. 5 (color online). *P*-wave spin splittings [energies relative to the spin average of the $\chi_b(1P)$ states] compared to experiment. Errors are statistical/fitting only and include the uncertainty in the determination of the lattice spacing. Large systematic errors are expected as discussed in the text.

3. D-wave spin-dependent splittings

Here, only the $\Upsilon_2(1D) - \eta_{b2}(1D)$ splitting was calculated using the E^{--} and T_2^{-+} representations, as these two states do not mix and can be computed from the same heavy-quark propagators.

The lattice results for the different ensembles are listed in Table IX. On the $am_l = 0.005$ ensemble, the splitting in physical units is found to be 1.8 ± 3.7 MeV where the error given is statistical/fitting only and includes the uncertainty from the determination of the lattice spacing. No experimental results are available.

IV. CONCLUSION

In this paper, a comprehensive calculation of the bottomonium spectrum with improved lattice NRQCD on the RBC/UKQCD $24^3 \times 64$, $L_s = 16$ gauge configurations with $2 + 1$ flavors of dynamical domain wall fermions was presented. The results are similar to those obtained in [14] with the same heavy-quark action from the coarse MILC gauge configurations, which use the AsqTad fermion action and the Lüscher-Weisz gluon action. In particular, good agreement with experiment was found for the radial and orbital energy splittings, for which systematic errors due to the NRQCD action are small. Furthermore, no significant deviations of the speed of light from 1 in the $\eta_b(1S)$ dispersion relation were found within the small statistical errors. The calculations in this work provide further evidence for the good properties of the domain wall and Iwasaki actions employed by the RBC and UKQCD Collaborations. By comparing the $2S - 1S$ radial energy splitting to experiment, independent determinations of the lattice spacings were performed, giving $a^{-1} = 1.740(25)_{\text{stat}}(19)_{\text{syst}}$ GeV for the most chiral ensemble.

The results for the fine and hyperfine structure are expected to have larger systematic errors due to missing radiative and relativistic corrections in the NRQCD action as well as discretization errors. Nevertheless, relatively good agreement with experiment was seen for the P-wave fine structure, and the deviation to experiment in the $1S$ hyperfine splitting was found to be much smaller than for the previous result obtained from a relativistic heavy-quark action in [10].

The calculations presented here are only for one lattice spacing. A more systematic analysis of discretization errors will be performed once new ensembles with a finer lattice spacing are made available by the RBC and UKQCD Collaborations.

Having obtained the bottomonium spectrum and the bare heavy-quark mass in this work, the next step is to perform calculations for heavy-light systems. Results for the spectrum of heavy-light baryons and mesons with domain wall valence quarks but with *static* heavy quarks were recently presented in [28]. Heavy-light computations with NRQCD heavy- and domain wall light valence quarks

on the same RBC/UKQCD gauge field ensembles are currently underway.

ACKNOWLEDGMENTS

[1] D. J. Antonio *et al.* (RBC and UKQCD Collaborations), Phys. Rev. D **75**, 114501 (2007).
[2] C. Allton *et al.* (RBC and UKQCD Collaborations), Phys. Rev. D **76**, 014504 (2007).
[3] D. J. Antonio *et al.* (RBC and UKQCD Collaborations), Phys. Rev. D **77**, 014509 (2008).
[4] C. Allton *et al.* (RBC and UKQCD Collaborations), Phys. Rev. D **78**, 114509 (2008).
[5] D. J. Antonio *et al.* (RBC and UKQCD Collaborations), Phys. Rev. Lett. **100**, 032001 (2008).
[6] P. A. Boyle *et al.*, Phys. Rev. Lett. **100**, 141601 (2008).
[7] D. B. Kaplan, Phys. Lett. B **288**, 342 (1992).
[8] Y. Shamir, Nucl. Phys. **B406**, 90 (1993).
[9] V. Furman and Y. Shamir, Nucl. Phys. **B439**, 54 (1995).
[10] M. Li (RBC and UKQCD Collaborations), Proc. Sci., LATTICE2008 (2008) 120.
[11] B. A. Thacker and G. P. Lepage, Phys. Rev. D **43**, 196 (1991).
[12] G. P. Lepage, L. Magnea, C. Nakhleh, U. Magnea, and K. Hornbostel, Phys. Rev. D **46**, 4052 (1992).
[13] C. T. H. Davies, K. Hornbostel, A. Langnau, G. P. Lepage, A. Lidsey, J. Shigemitsu, and J. H. Sloan, Phys. Rev. D **50**, 6963 (1994).
[14] A. Gray, I. Allison, C. T. H. Davies, E. Dalgic, G. P. Lepage, J. Shigemitsu, and M. Wingate, Phys. Rev. D **72**, 094507 (2005).
[15] E. Dalgic, J. Shigemitsu, and M. Wingate, Phys. Rev. D **69**, 074501 (2004).
[16] G. P. Lepage and P. B. Mackenzie, Phys. Rev. D **48**, 2250 (1993).
[17] R. C. Johnson, Phys. Lett. **114B**, 147 (1982).
[18] G. P. Lepage, B. Clark, C. T. H. Davies, K. Hornbostel, P. B. Mackenzie, C. Morningstar, and H. Trottier, Nucl. Phys. B, Proc. Suppl. **106–107**, 12 (2002).
[19] B. Aubert *et al.* (*BABAR* Collaboration), Phys. Rev. Lett. **101**, 071801 (2008); **102**, 029901(E) (2009).
[20] C. Amsler *et al.* (Particle Data Group), Phys. Lett. B **667**, 1 (2008).
[21] G. Bonvicini *et al.* (CLEO Collaboration), Phys. Rev. D **70**, 032001 (2004).
[22] C. T. H. Davies, K. Hornbostel, G. P. Lepage, A. Lidsey, P. McCallum, J. Shigemitsu, and J. H. Sloan, Phys. Rev. D **58**, 054505 (1998).
[23] Y. Iwasaki, Report No. UTHEP-118, 1983.
[24] Y. Iwasaki and T. Yoshie, Phys. Lett. **143B**, 449 (1984).
[25] S. Necco, Nucl. Phys. **B683**, 137 (2004).
[26] C. T. H. Davies *et al.* (HPQCD, UKQCD, MILC, and Fermilab Lattice Collaborations), Phys. Rev. Lett. **92**, 022001 (2004).
[27] *Quarkonia*, edited by W. Buchmüller, Current Physics—Sources and Comments Vol. 9 (North-Holland, Amsterdam, 1992).
[28] W. Detmold, C. J. Lin, and M. Wingate, arXiv:0812.2583.
[29] R. G. Edwards and B. Joo (SciDAC, LHPC and UKQCD Collaborations), Nucl. Phys. B, Proc. Suppl. **140**, 832 (2005).